Research on comprehensive assessment and prediction method of slope stability based on multivariate coupled model of vibration loading

Abstract: The study of slope dynamic response and slope stability under different vibration conditions is of great significance to the slope design in engineering, safe operation of engineering construction equipment and safe prediction of vehicle stopping. This paper combines the relevant factors affecting the deformation and damage of slopes, and establishes a three-dimensional model of slopes for similar simulation using actual engineering slopes. With the advantage of the finite element strength reduction method, the stability of the slope under different vibration loads and the minimum safety factor are solved. Investigate the nodal properties of the slopes in the study area, and the values of shear strength c and φ of the structural surface of the slopes. Simulate and analyze the longitudinal and transverse waves under vibration loads. Trace the slope nodes and analyze the dynamic response of the slope under vibration loading. Explore the sensitivity of the factors affecting the slope stability under vibration loading, and make an overall evaluation of the slope stability. In the dynamic response curves, the horizontal and vertical stress curves tend to zero after 0.73-1.4s at monitoring points No. 1 and No. 2. That is, the vibration duration is about 0.73-1.4s, which is also consistent with the duration obtained from the on-site blasting vibration test. 1# and 2# monitoring points, the initial stress is larger. And the mass vibration of signal #2 is stronger than that of signal #1, but the main vibration frequency of signal #1 is much higher than that of signal #2. In these two signals, the frequency is the dominant factor in destroying the slope. The comprehensive assessment result is that under the action of blasting load (Case II), the rock mass in Area I is in an unstable state, and Area II is in a stable state.

Keywords: strength discounting method; shear strength; vibration loading; slope stability

1. Introduction

Every year in the construction of highways and railroads, many slopes need to be excavated, and their stability is an important influence on whether the project can be completed on schedule [1-2]. The stability of natural slopes is determined by the engineering geology, hydrogeology and geotechnical properties of the constituent slopes, and the slopes filled and excavated artificially, such as pits, ditches, embankments, earth dams, etc. are usually called artificial slopes, whose stability is affected by the quality of the construction, groundwater, soil properties, and so on. Therefore, there are more factors affecting the stability of slopes, among which some factors with ambiguity inevitably exist [3-5].

The consequences of geologic hazards caused by slope instability are often difficult to estimate, and a small one can block traffic and cause economic losses, while a large one can lead to casualties [6-7]. Therefore, how to accurately evaluate the stability of slopes seems to be crucial, and the decision-making of the management program after the stability evaluation is the most important factor for the success of management. The evaluation of slope stability is a discrete, random, nonlinear and complex problem [8-9]. And how to express the influence factors with fuzzy nature is also a problem worth studying. Many scholars have done a lot of research on the evaluation of slope stability and proposed many evaluation methods, most of these methods have certain limitations, some of which can not accurately describe the fuzzy nature of slopes, and some of which have deficiencies in the calculation [10-11]. In conclusion, accurate evaluation of slope stability is a prerequisite for the decision-making of slope management program, and the decision-making of management program is a key factor related to the success of slope management [12].

Slope stability analysis has been one of the important research topics in the field of geotechnical engineering [13]. At present, the limit equilibrium theory is the most commonly used in actual engineering, based on just limit equilibrium theory of

various types of strip partitioning method is simple to calculate, the development is relatively perfect, and in practice, a large number of experience, more widely used in engineering. However, the drawbacks of this type of method are also obvious, that is, it is unable to consider the kinematics of slope damage, so there are inevitable errors in the stability analysis [14-15].

In this paper, based on the existing application of numerical simulation in slope stability and the judgment basis of slope dynamic stability, the vibration load solution formula is used to establish a three-dimensional model of slope stability. The construction stage simulation is carried out by using the strength discount method to solve the stability problems of slopes under different working conditions and the slope safety and stability coefficients. Statistical study area slope structural surface shear strength parameters, analyze the destruction mechanism of the slope structural surface rock layer under the action of blasting load. Simulate the input of vibration load and analyze the dynamic response process of slope monitoring points. Explore the sensitivity of factors affecting slope stability under vibration loading. Classify the slope stability state and carry out the grade evaluation of slope stability.

2. Basis for integrated slope stability assessment

Stability analysis of fill slopes and excavated slopes is a relatively common study in geotechnical analysis. The self-weight of the slope body itself, pore water pressure, additional load stress, and fluctuating water pressure load stress have a great influence on the stability of the slope body. When the slope itself under the action of self-weight and additional external loads, the shear stress generated inside the slope body is greater than the shear strength of the slope soil body, the slope will appear damage phenomenon. Slope stability analysis is the shear stress and shear strength to study and analyze the calculation of slope stability problems [16-18].

The following calculation methods are generally recommended for slope stability analysis:

An overall analysis method based on the theory of slope limit equilibrium and the method of strip partition analysis.

A limit analysis method based on slope strength theory.

A finite element analysis method based on slope elasticity theory.

Safety management of slopes not only needs to be clear about the minimum safety factor of the slope, but also needs to analyze the slope morphology. In this way, monitoring points can be set at appropriate locations to obtain valuable monitoring information. The Finite Element Method (FEM) can provide the required data and can analyze the damage process of the slope.

The MIDAS/GTS method of slope analysis is a strength reduction method utilizing the finite element method.

2.1 Factors affecting the deformation and damage of slopes

2.1.1 Degree of penetration of the controlling structural surfaces

In rocky slopes, the structural surface is one of the important factors causing deformation and damage to the slope. The joints and fissures within the slope are very developed, the joint spacing is small, and most of the structural surfaces are open and filled with mud film or no filling. In the process of unloading the slope to the critical direction, the structural surface within the rock body gradually expands and extends until it penetrates, constituting the rear boundary of the slope rock body destabilization.

2.1.2 Weathering unloading

Weathering of the slopes will reduce the quality of the rock mass and exacerbate the differential weathering of sandstone and mudstone. It will also reduce the mechanical properties of the structural surface. The unloading of the slope to the critical direction will cause the rock mass at the top of the slope to be tensile and open, forming tensile fissures that tend to be out of slope and rough and undulating. At the

same time, it will also make the rock body has formed the tensile fissure and shear joints further extension, expansion or even through. It can be seen that under the action of various natural camping forces, the weathering unloading of the slope reduces the stability of the rock mass.

2.1.3 Natural factors such as heavy rainfall and earthquakes

The rainfall in the study area is more concentrated and the amount of single rainfall is larger. Rainfall infiltration into the slope body can, on the one hand, soften the structural surface and reduce the mechanical properties. On the other hand, it will also make the pore water pressure in the fissures rise, generating hydrostatic pressure and dynamic water pressure, forcing the expansion of the original fissures in the rock mass and the movement of the rock mass in the direction of the proximity, which is not conducive to the stability of the slope.

If there are weak structural surfaces such as muddy siltstone and carbonaceous shale developed in the rock body of the slope, its strength can be significantly reduced under the long-term action of rainwater. In addition, a large number of open structural surfaces developed in sandstone provide a good channel for surface water infiltration. Therefore, under rainfall conditions, the slope is prone to slope instability. Earthquake, as a sudden natural disaster, has a very important impact on slope stability.

The impact of earthquakes on the stability of the slope rock mass is manifested in two aspects: cumulative effect and triggering effect. The former is mainly manifested in the loosening of slope rock structure caused by seismic action, rupture surface, weak surface dislocation and pore water pressure cumulative rise and so on. The latter is mainly manifested in the role of the earthquake to make in the critical state or at present although in the basic state of stability, but in the unfavorable combination of load is easy to destabilize the slope instantly destabilized.

2.1.4 Construction blasting and train vibration loads

The development and evolution of natural slopes is a process of gradual

stabilization. Human engineering activities have interfered with or even destroyed the original development and evolution trend of the slope, resulting in the stress differentiation of the slope rock mass and the concentration of shear stress near the foot of the slope. In the vicinity of the slope shoulder, under certain conditions, the radial stress of the slope surface is transformed into tensile stress, forming a tension zone, which is prone to tensile crack damage. In the process of tunnel excavation in the slope, the vibration load caused by construction blasting is extremely unfavorable to the stability of the slope and dangerous rock body. At the same time, in the process of railroad line operation, the vibration load of the train also has an unfavorable impact on the stability of the slope.

2.2 Application of numerical simulation in slope stability analysis

With the rapid development of computer technology, numerical simulation is widely used in various research fields. The emergence of numerical simulation gives the stability analysis of slopes a broader development prospect. By establishing a mathematical model relatively close to reality and combining relevant knowledge and theory, it is easy to show the process of slope deformation bad. It helps to understand the mechanism of slope destabilization.

At the same time, the reliability of the simulation can also be compared through experimental studies on the slope stability analysis of several commonly used simulation methods including the finite element method, boundary element method and discrete unit method. Compared with other methods, the finite element method is more widely used due to its practicality and accuracy.

The basic idea of the finite element method is used to solve the region by a finite set of discrete and somehow combined units assembled to represent the entire solution domain and the unknown field function in pieces with the approximation function assumed within each unit.

The approximate function within a cell is usually expressed by the values of the

unknown field function and its derivatives at each node of the cell and its interpolating function. The value of the unknown field function or its derivative at each node becomes the new unknown quantity (degree of freedom), thus turning a continuous infinite degree of freedom problem into a discrete finite degree of freedom problem.

As the number of cells increases, i.e., the cell size is reduced, the approximation of the solution is continuously improved, and if the cell convergence conditions are satisfied, the approximate solution converges to the exact solution. The finite element method is widely used in numerical simulation because of these characteristics, and has become an important means of solving the numerical simulation of blasting.

3. Vibration loads on slope stability

3.1 Finite element strength discounting method

In the traditional sense, the slope limit equilibrium method first sets up a slip surface and calculates the stability coefficient based on the force or moment equilibrium, which is defined as the ratio of the slip resistance or moment of the slope slip surface to the sliding force or moment:

$$K = \frac{\int_0^1 \tau_f dl}{\int_0^1 \tau dl} = \frac{\int_0^1 (c + \sigma_n \tan\varphi) dl}{\int_0^1 \tau dl} \tag{1}$$

Where, K is the safety factor. τ_f is the shear strength on the sliding surface. τ is the actual strength at each point on the sliding surface. Dividing both sides of the above equation by K gives:

$$1 = \frac{\int_0^1 (\frac{c}{K} + \sigma_n \frac{\tan\varphi}{K}) dl}{\int_0^1 \tau dl} = \frac{\int_0^1 (c' + \sigma_n \tan\varphi') dl}{\int_0^1 \tau dl} \tag{2}$$

$$c' = \frac{c}{K}, \tan\varphi' = \frac{\tan\varphi}{K} \tag{3}$$

As in the above equation, the left side of the equation is equal to 1, which means

that when the strength is reduced to K, the mechanical state of the slope reaches the limit, i.e., the slope reaches the state of destruction, and K is the safety coefficient obtained by the strength reduction method.

Numerical calculation set a number of discount coefficient, and then according to the set value calculation to get the discount strength parameters, from these parameters for numerical analysis, constantly increase the value of K for calculation, to observe its convergence, to the critical state when the discount coefficient is the slope stability coefficient.

3.1.1 Advantages of the strength reduction method

The method has the advantages of both traditional limit analysis and numerical computational analysis, which can conform to the practical characteristics of geotechnical actual engineering as well as the characteristics of wide practicality of numerical analysis.

(1) The finite element strength reduction method is different from the traditional method in that there is no need to divide the bars and set the slip surface, but to find out the sliding surface and the safety and stability coefficient according to the set program.

(2) The nonlinear stress-strain relationship of soil body can be considered in the calculation of finite element reduction, which can reflect the actual problems of slope engineering more closely.

(3) This method has some advantages of numerical calculation methods, and gets rid of the shortcomings of traditional methods limited to the slope geometry and material inhomogeneity, etc., so that numerical calculations can be carried out for the projects with complex geological environment conditions.

(4) The finite element strength reduction method can consider the stress-strain ontological relationship, and the calculation results can provide more comprehensive information such as soil displacement change and plastic deformation zone.

(5) For more complex slope projects, this method can calculate the effect of

slope and support structures and construction excavation and other processes.

3.1.2 Slope dynamic stability criteria

When the slope is in static state and the stability is analyzed by numerical analysis, the following methods are usually used to judge whether it is stable or not:

(1) In finite element analysis, the convergence or not of the calculation process is usually taken as the evaluation standard of slope stability. When the program calculation does not converge, it is considered to reach the unstable state.

(2) Take the sudden change of displacement and the inflection point of displacement curve as the evaluation standard, when the slip surface or displacement changes suddenly, it is considered to reach the instability state.

(3) Whether the plastic zone forms a connected area is taken as the evaluation criterion. In the process of discount calculation, if the plastic zone appears to be connected from the foot of the slope to the top of the slope, it is considered that the instability state is reached.

The first two of the above three judgments are not converged in the numerical calculation process, but the third one does not necessarily lead to slope damage, which is only a necessary condition for slope instability. Therefore, in the numerical simulation of finite element, the non-convergence of the calculation is generally used as the discriminating condition when the displacement changes abruptly, and the third one is analyzed and studied at the same time.

Stability analysis of the slope under dynamic conditions is similar to the static situation, but the dynamic analysis of the load size and direction is changing, which will make the displacement will change. Therefore, when there is a sudden change in displacement, it is not necessarily a destructive state. When there is obvious displacement mutation can be used as a criterion, when it is not obvious, the three criteria will be analyzed in combination.

3.2 Vibration loads

The vibration load calculation is mainly coupled with the results of the system dynamics simulation and analysis, and the power spectral density function can only be directly inputted when the linear random vibration frequency domain analysis is performed. And for nonlinear random vibration analysis, the most effective method is the numerical integration method [19-20].

The coupled dynamics equations of the system can be expressed uniformly in matrix form as:

$$[M]\{\ddot{X}\}+[C]\{\dot{X}\}+[K]\{X\}=\{P\} \tag{4}$$

where $[M]$ is the generalized mass matrix. $[C]$ is the generalized damping matrix, $[K]$ is the generalized stiffness matrix. $\{\ddot{X}\},\{\dot{X}\},\{X\}$, respectively, is the generalized acceleration, generalized velocity, and $\{P\}$ is the generalized force vector matrix.

In fact, when the vibration load is operated, the inertial force, damping characteristics and elastic force characteristics of the system are constantly changing, and as a result, all $[M],[C],[K]$ of the system are constantly changing with time. In addition, equation (4) has time-varying characteristics. In this paper, a stepwise integration method will be used to solve the system dynamics equations in order to obtain the time domain solution of the system.

There are various forms of stepwise integration methods, and in this paper, the Wilson-θ method is used for the stepwise integration of the system dynamics differential equations. This method, when the integration parameters are appropriately determined, ensures the unconditional stability of the algorithm and allows the computational results to reach a high degree of accuracy.

The Wilson-θ method is an integration method that can achieve unconditional stability and is a generalization of the linear acceleration method. The expression for its acceleration in $[t,t+\Delta t]$ time is:

$$\ddot{X}(t+\tau)=\ddot{X}(t)+\frac{\tau}{\theta\Delta t}\left[\ddot{X}(t+\theta\Delta t)-\ddot{X}(t)\right] \tag{5}$$

where $\theta>1$, in order to ensure unconditional stability, holds only when $\theta>1.37$. Usually $\theta=1.40$ is taken in general programs, and is obtained by integrating the equation:

$$\dot{X}(t+\tau)=\dot{X}(t)+\ddot{X}(t)\tau+\frac{\tau^2}{2\theta\Delta t}\left[\ddot{X}(t+\theta\Delta t)-\ddot{X}(t)\right] \tag{6}$$

$$X(t+\tau)=X(t)+\dot{X}(t)\tau+\frac{1}{2}\ddot{X}(t)\tau^2+\frac{\tau^3}{6\theta\Delta t}\left[\ddot{X}(t+\theta\Delta t)-\ddot{X}(t)\right] \tag{7}$$

Let $\tau=\theta\Delta t$, i.e., at moment $t+\theta\Delta t$ there is:

$$\dot{X}(t+\theta\Delta t)=\dot{X}(t)+\frac{\theta\Delta t}{2}\left[\ddot{X}(t+\theta\Delta t)+\ddot{X}(t)\right] \tag{8}$$

$$X(t+\theta\Delta t)=X(t)+\dot{X}(t)\partial\Delta t+\frac{\theta^2\Delta t^2}{6}\left[\ddot{X}(t+\theta\Delta t)+2\ddot{X}(t)\right] \tag{9}$$

From the above two equations the velocity and acceleration at moment $t+\theta\Delta t$ can be solved, i.e.:

$$\ddot{X}(t+\theta\Delta t)=\frac{6}{\theta^2\Delta t^2}\left[X(t+\theta\Delta t)-X(t)\right]-\frac{6}{\theta\Delta t}\dot{X}(t)-2\ddot{X}(t) \tag{10}$$

$$\dot{X}(t+\theta\Delta t)=\frac{3}{\theta\Delta t}\left[X(t+\theta\Delta t)-X(t)\right]-2\dot{X}(t)-\frac{\theta\Delta t}{2}\ddot{X}(t) \tag{11}$$

The expression for moment $t+\theta\Delta$ in Eq:

$$M\ddot{X}(t+\theta\Delta t)+C\dot{X}(t+\theta\Delta t)+KX(t+\theta\Delta t)=P(t+\theta\Delta t) \tag{12}$$

Among them:

$$\overline{P}(t+\theta\Delta t)=P(t)+\theta\left[P(t+\Delta t)-P(t)\right] \tag{13}$$

The equation about $X(t+\theta\Delta)$ is obtained as:

$$\begin{aligned}&\left(K+\frac{6}{\theta^2\Delta t^2}M+\frac{3}{\theta\Delta t}C\right)X(t+\theta\Delta t)\\&=P(t)+\theta\left[P(t+\Delta t)-P(t)\right]\\&+M\left[\frac{6}{\theta^2M^2}X(t)+\frac{6}{\theta\Delta t}\dot{X}(t)+2\ddot{X}(t)\right]\\&+C\left[\frac{3}{\theta\Delta t}X(t)+2\dot{X}(t)+\frac{\theta\Delta t}{2}\ddot{X}(t)\right]\end{aligned} \tag{14}$$

Remember $\tilde{K} = K + \frac{6}{\theta^2 \Delta t^2} M + \frac{3}{\theta \Delta t} C$.

$$\begin{aligned} \tilde{P}(t+\theta\Delta t) = P(t) + \theta\left[P(t+\Delta t) - P(t)\right] \\ + M\left[\frac{6}{\theta^2\Delta t^2} X(t) + \frac{6}{\theta\Delta t}\dot{X}(t) + 2\ddot{X}(t)\right] \\ + C\left[\frac{3}{\theta\Delta t} X(t) + 2\dot{X}(t) + \frac{\theta\Delta t}{2}\ddot{X}(t)\right] \end{aligned} \tag{15}$$

The formula can be written as:

$$\tilde{K}X(t+\theta\Delta t) = \tilde{P}(t+\theta\Delta t) \tag{16}$$

Solving the above equation gives $X(t+\theta\Delta t)$. Substituting the obtained $X(t+\theta\Delta t)$ into (14) gives $\ddot{X}(t+\theta\Delta t)$. If $\tau = \Delta t$ is obtained in equation (15) and substituting it into (16):

$$\ddot{X}(t+\Delta t) = \frac{6}{\theta^3\Delta t^2}\left[X(t+\theta\Delta t) - X(t)\right] - \frac{6}{\theta^2\Delta t}\dot{X}(t) + (1-\frac{3}{\theta})\ddot{X}(t) \tag{17}$$

where $\tau = \Delta$ is taken to have:

$$\ddot{X}(t+\theta\Delta t) - \ddot{X}(t) = \theta\left[\ddot{X}(t+\Delta t) + \ddot{X}(t)\right] \tag{18}$$

Substituting the above equation into (17) and (18) and taking $\tau = \Delta t$ has:

$$\dot{X}(t+\Delta t) = \dot{X}(t) + \frac{\Delta t}{2}\left[\ddot{X}(t+\Delta t) + \ddot{X}(t)\right] \tag{19}$$

$$X(t+\Delta t) = X(t) + \Delta t\dot{X}(t) + \frac{\Delta t^2}{6}\left[\ddot{X}(t+\Delta t) + 2\dot{X}(t)\right] \tag{20}$$

3.3 Numerical modeling

3.3.1 Three-dimensional modeling

In this paper, a 3D model of the slope is established based on the actual engineering slope for similar simulation. Based on repeated on-site exploration and observation of the topographic map of the entire slope, the elevation is marked in AutoCAD and imported into Midas-GTS/NX, three rock and soil layers of different materials are established, and a 3-dimensional model with 1:1 ratio with the original slope is formed for analysis. The modeling principle utilized is the strength discount

method. Stress, strain and displacement of the landslide are analyzed through simulation, and the stability coefficient of the slope and the potential sliding surface of the hazardous area can be obtained by analyzing the cloud diagram.

The model simulates the distribution of the rock and soil layers in 3D form, and the damage discrimination mode selects the Moore-Cullen criterion to establish a 3D slope model. The slope model is divided into three layers, namely, pulverized yellow clay, mudstone and tuff, and constraints are imposed to make the numerical simulation model converge. The constraints are chosen to be applied on the left and right sides of the solid 3D slope model and the bottom surface of the slope, the rest of the slope surface is left free without any external force and only the gravity of the slope is attached under natural conditions.

3.3.2 Grid Division and Boundary Conditions

During the meshing process, Midas-GTS/NX generally refines the mesh and utilizes differentials to observe slope changes in areas where the model is focused for discussion and study. When dividing different grid sizes, the program provides methods such as "Unit Length", "Number of Divisions", "Linear Gradient (Length)", "Linear Gradient (Ratio)" to control the mesh size of the corresponding lines. Regardless of the method used, the meshes that have been delineated are adapted to the neighboring meshes. In this paper, we use the unit length method to divide the grid and refine the part of the slope near the slope face. The DXF file of the slope model is imported into Midas-GTS/NX. Then it was expanded into a 3D model with a thickness of 20 m. The expanded solid model was meshed according to the specified line unit length, and the model grid included 8757 nodes and 8783 grid cells. The nodal surface structure of the slope is an important unit in the modeling, and Midas slope simulation software can realize the definition of the slope down-layer tendency nodal by adjusting the parameters of the nodal surface in the material selection.

In this paper, the strength reduction method, which has a high degree of credibility at present, is used to carry out the simulation of the construction phase,

which in turn solves the stability problem of slopes under various working conditions and the slope safety and stability coefficients. The method involves initial ground stresses, which will affect the calculation results. Therefore, to converge the model for numerical simulation, constraints are imposed on it. The constraints are chosen to be applied on the left and right sides of the solid 3D slope model as well as on the bottom surface of the slope, leaving the rest of the slope surface in a free state without applying any external forces and ensuring that only the gravity of the slope is attached under natural conditions. In this paper, the gravitational acceleration is only applied in the initial calculation step. In addition, there are high demands on the model, which require the imposition of boundary conditions. The selected representative slope sections of the 3D model where blasting and vibrometry are performed during production blasting operations are simulated.

3.3.3 Principles of analysis of fractured rock formations under vibration loading

Under the action of blasting loads, the down-layer slope is prone to structural surface fragmentation and then produce slip - pull crack damage, structural surface damage will occur slope rock bite and friction decline and then produce instability potential, the specific mechanical equilibrium formula is as follows:

$$F_{S\times}=\frac{R}{S}=\frac{\sum\left\{cl_1+\left[\left(F_X+H-V\right)\sin\theta+G\cos\theta\right]\tan\varphi\right\}}{\sum\left[G\sin\theta-\left(F_X+H+V\right)\cos\theta\right]} \tag{21}$$

$$F_{SZ}=\frac{R}{S}=\frac{\sum\left\{cl_1+\left[\left(G-F_Z\right)\cos\theta+\left(H-V\right)\sin\theta\right]\tan\varphi\right\}}{\sum\left[\left(G-F_Z\right)\sin\theta-\left(H+V\right)\cos\theta\right]} \tag{22}$$

Where G is the self-gravity force of the damaged rock. l_1 is the length of the damaged surface, c is the cohesive force, and φ is the angle of internal friction.

4. Numerical analysis of the stability of rocky slopes under vibratory loading

4.1 Engineering investigation of slopes in the study area

West-Shanghai Expressway Lantian East-Qinling South Section, this section of the highway is generally located in the mountainous area along the watershed of the main ridge of the Qinling Mountains. In addition to Shangluo, the relatively flat and rocky low mountains in the territory are dominant, with an altitude of 700-2000 meters and a relative height difference of 300-1200 meters. In the geological structure in the Qinling fold and the Qinling Garidong fold belt on the transition zone. The topography of the area is highly undulating, with the overall terrain high in the middle and low in the east of the north and west of the south. The spreading of the mountain ranges and grooves is controlled by the tectonic belt of the Qinling Mountains, and the mountains are large and deep, with a complicated topography. The terrain in the Ba River area is steep, mostly characterized by gorges, with the main river valleys dominated by “S” valleys, and the valleys in the Qinling Mountains are mostly “V” valleys, which are more intensely cut, and there are a number of different types of rocky slopes along the tunnel design line.

(1) K51+899.6 Tunnel Portal Slope/Area I

The slope is located in the fifth group of Fengjiawan Village, Jiumafang Township, Lantian County, with a maximum slope height of 50 meters and a maximum depth of 60 meters, which is relatively shallow. The bedrock is exposed and the rock body is developed with weathering fissures near the surface.

This survey statistically analyzed the nodules, and there were three main types of nodules. The nodules are 73° ∠ 64° with a frequency of 5 bars/m, 321° ∠ 60° with a frequency of 1.1 bars/m, and 120° ∠ 60° with a frequency of 2.5 bars/m. All of them are shear joints with long extensions. Small amounts of calcite are seen filling the joints. Weathering fissures are more developed in the near-surface rock body.

The stratum distributed in the tunnel site area is Yanshan early granite, which is described as follows according to its stratigraphic age and degree of weathering:

①Strongly weathered granite: the rock body is divided into rubble by weathering fissures, the fissure surface can be seen as rust-colored infiltration, attached to clay particles, the hammering sound is dumb and easy to be crushed, Vp =1800~2500m/s, the thickness is about 6~10m.

②Medium weathering granite: light gray mainly, granite patchy structure, block structure. The hammering sound is brittle and not easy to break. Vp =2350~3100m/s.

③ slightly weathered granite: light gray mainly, granite mottled structure, block structure. The hammering sound is brittle and not easy to break. Vp =2800~3500m/s.

The slope of the tunnel portal is located at the slope of the mountain on the left bank of the river. According to the mapping data, the slope of the terrain is steep, and the slope angle is about 52°. The lithology is strongly weathered granite, joints are developed, and the rock body is prone to collapse along the joint surface. The tunnel site is located in a volcanic rock area with no fold output.

(2) Ba River No. 2 Tunnel Portal Slope/Area II

The slope is located in Hulu Fork Village, Lantian County, with a maximum slope height of 42 meters and a maximum depth of 62.24 meters, which is relatively shallow. The tunnel site area is a tectonically denuded middle mountainous area, and the tunnel side slopes are nearly perpendicular to the mountain. After mapping, there are mainly two groups of joints in the inlet section. The joints are 59° ∠ 70° with a frequency of 2 joints/m and 150° ∠ 35° with a frequency of 1.6 joints/m, all of which are shear joints.

The stratigraphy of the tunnel site is Huarixi quartz diorite, which is described as follows according to its stratigraphic age and degree of weathering:

① Strongly weathered quartz diorite: dominated by light gray, minerals are mainly feldspar and quartz. Vp =1900~2400m/s, thickness about 5~10m.

②Medium weathering quartz diorite: mainly light gray, granular porphyritic

structure, block structure, minerals mainly feldspar, quartz, mica and other dark minerals, joints and fissures are more developed. The sound of hammering is brittle and not easy to break. Vp=2680~3300m/s.

③Weathered quartz diorite: light gray mainly, granite porphyry structure, block structure, minerals mainly feldspar, quartz, see mica and other dark minerals, joints and fissures are not very developed. The hammering sound is brittle and not easy to break. Vp=3400~3600m/s.

4.2 Statistical Analysis of Shear Strength Parameters of Structural Surfaces of Slopes

According to the previous analysis, it can be seen that the main factors affecting the rocky slopes under dynamic loading are the c and φ values of the rock mass gravity, the shear strength of the structural surface. And the influence of the thickness of the cover layer. According to the field investigation sampling and indoor test statistical analysis data, the shear strength index value and physical mechanical parameters of the slope are obtained.

The statistics of shear strength index and physical mechanical parameters of slopes in Area Ⅰ are shown in Table 1. N and S in the table represent natural and saturated respectively.

Table 1 Slope shear strength index and mechanical parameter statistics

Serial number	Categories	Severity(γ) kN/m^3		Elastic modulus $(E)MPa$	Poisson ratio (μ)	Cohesion $(C)kPa$		Interior friction Angle(φ)	
		Nature	Saturation			N	S	N	S
1	Blanket clay	21.24	25.08	15	0.415	82	43	15.36	12.12
2	Gravel clay	20.06	23.41	31	0.369	43	46	18.04	17.07
3	Rubble clay	23.69	25.66	45	0.344	53	41	21.69	19.52

4	Strong wind	23.02	24.71	63	0.358	65	59	41.31	39.61
5	Stroke rock	23.12	25.19	97	0.374	69	63	44.12	42.79
6	Breezy rock	25.76	25.83	92	0.391	71	64	47.65	42.53

The statistics of shear strength index and physico-mechanical parameters of slopes in Zone II are shown in Table 2.

Table 2 Analysis of shear strength indexes and physical mechanical parameters

Serial number	Categories	Severity(γ) kN/m^3		Elastic modulus (E) MPa	Poisson ratio (μ)	Cohesion (C) kPa		Interior friction Angle(φ)	
		Nature	Saturation			N	S	N	S
1	Gravel clay	20.06	23.41	31	0.369	43	46	s	17.07
2	Rubble clay	23.69	25.66	45	0.344	53	41	21.69	19.52
3	Strong wind	23.02	24.71	63	0.358	65	59	41.31	39.61
4	Stroke rock	23.12	25.19	97	0.374	69	63	44.12	42.79

4.3 Measurement and calculation of the elevation and coordinates of the original landform of the slope

Due to the physical and chemical effects of erosion and weathering of the original slope cover and exposed bedrock, the original geomorphology has changed to a certain extent. In order to accurately modeling needs, as far as possible to restore the real geomorphological situation.

For this reason, after the field conductor re-survey, based on the original survey data of the Xishang Expressway, and on the basis of the original coordinates of the advanced control points, the elevation of the location of typical slopes was re-established. The contour file was drawn, and the survey points were arranged in the sampling point part of the typical slope. One measuring point is set every 5 meters, and the setting of measuring points can be encrypted according to the needs, and the

surface elevation of the reset slope is shown in Table 3.

Table 3 The slope is the relative height of the slope

Measuring point	1	2	3	4	5	6	7	8	9
1	95.3	94.2	96.1	96	97.4	105	106	110	101
2	91.7	93.5	97	94.1	95.5	96.4	102	101.4	116
3	92	93.4	96.4	93.5	94.1	93.5	95.3	115.1	114
4	92.3	96.5	98.3	101	102.1	96	110.4	116.5	120.4
5	97.5	92.8	97.1	102	105.7	96.5	115.3	102	119.6
6	94.1	94.3	99.4	111	108.3	99	116.7	132	125.3
7	93.5	96.5	102	104.5	109.4	96.5	101.5	95.6	126.7
8	94.6	97.3	101	101.4	110.8	113.4	108.3	96.7	117.5
9	95	99	113.4	99.4	114.3	113.4	117.6	97.2	121.6
10	96	103.4	97.5	98.3	117.4	112.4	121.3	93.4	117.4
11	97.5	101	111.1	96.4	109.6	107.3	114.5	95.5	124.6
12	98	105.2	98.3	95.6	108.7	109	117.4	96.7	121.5

4.4 Load Simulation and Input

In the simulation of vibration, the load type used is seismic load. In the load simulation, according to the existing blasting site vibration load acquisition based on the vibration load processing, in the vibration meter to monitor the waves obtained for the P-wave and S-wave. Therefore, for the simulation of vibration load is the simulation analysis of the P wave and S wave, respectively, the first blasting vibration of the vibration tester P wave and S wave time curve shown in Figure 1.

The maximum value of the amplitude of the longitudinal wave is 2.7805cm/s, the main frequency of vibration is 20.1594Hz, and the vibration time is 1.0367s. The maximum value of the amplitude of the transverse wave is 2.5632cm/s, the main frequency of vibration is 16.0075Hz, and the vibration time is 1.0686s.

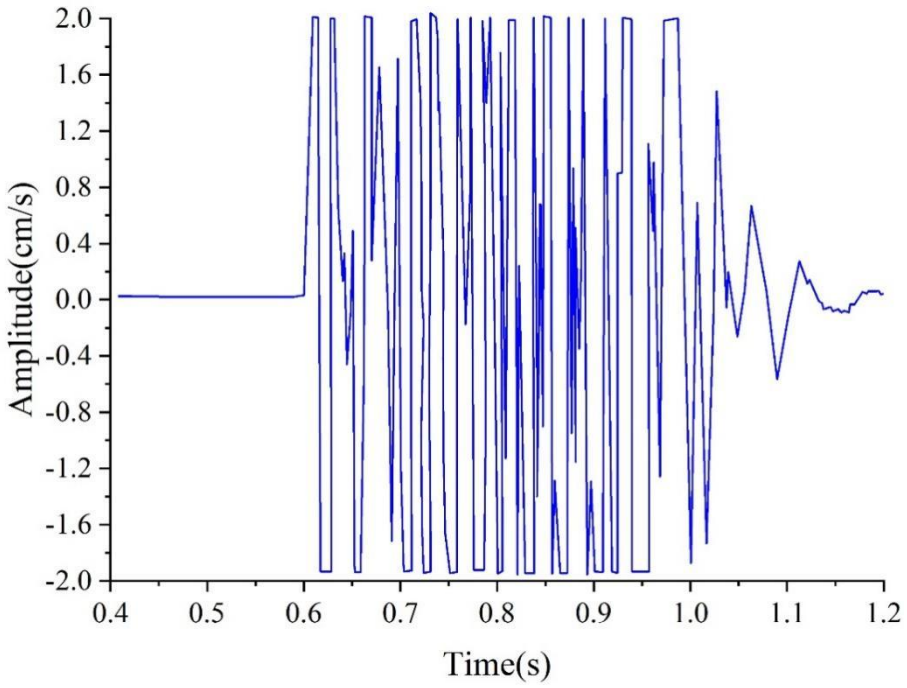

(a) P wave vibration velocity- Time relationship

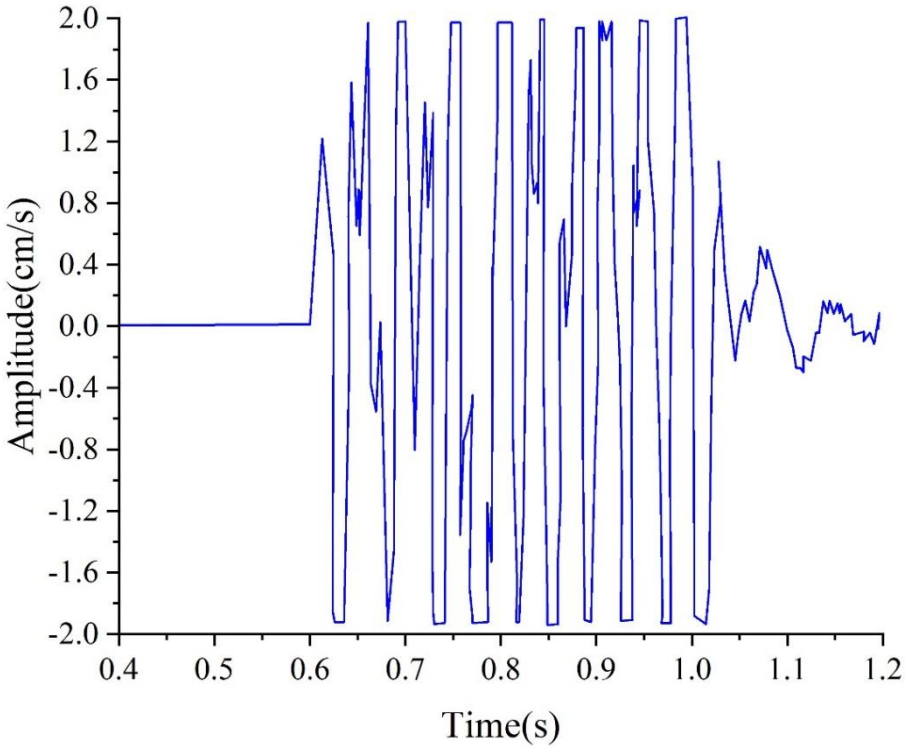

(b) S wave vibration velocity- Time relationship

Figure 1 The vibration tester p wave and s wave time curve of the first blasting vibration

In the processing of the simulated vibration wave, the segmented sinusoidal function is used to approximate the velocity-time curve instead of the blasting

vibration. In the input of the load, according to the acquisition characteristics of the vibrometer is used to input the longitudinal wave perpendicular to the direction of the top surface of the slope, and the transverse wave parallel to the direction of the slope.

The processed P and S wave velocity-time curve is shown in Fig. 2, and the rest of the blasting follows this principle.

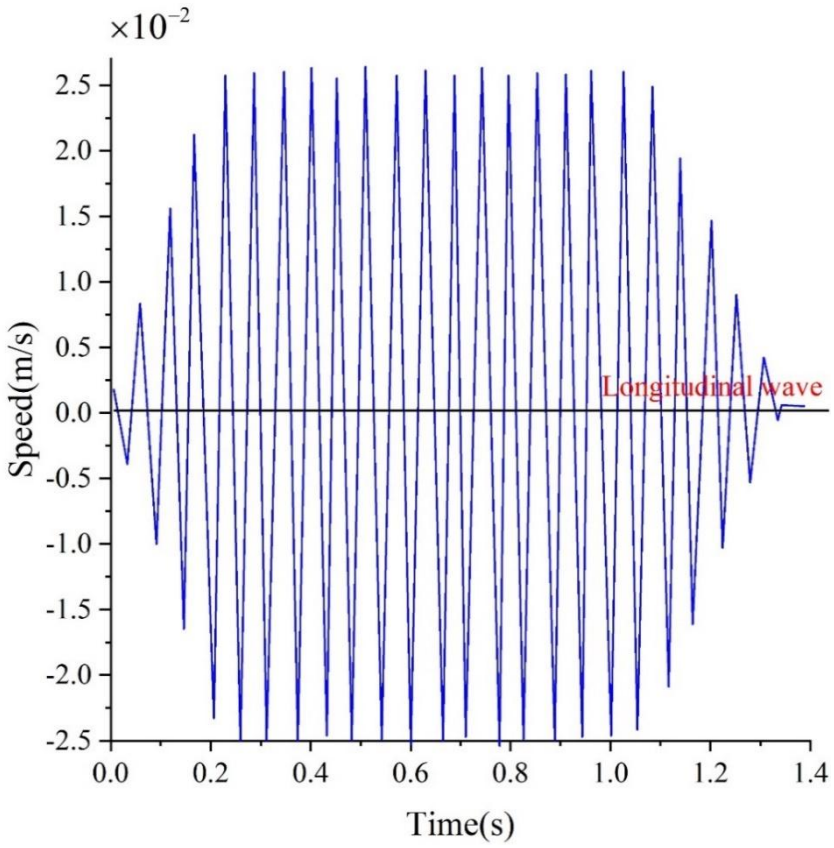

(a) Processed longitudinal velocity- Time relationship

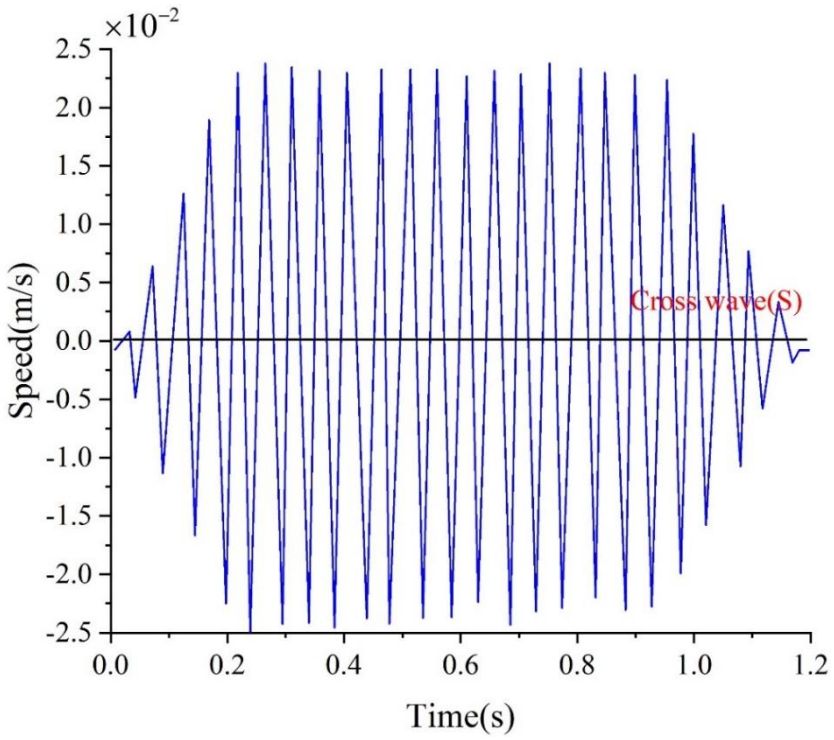

(b) Cross wave velocity- Time relationship

Figure 2 Processed velocity - time relationship

4.5 Dynamic response

Blast load was applied to the slope body on the basis of self-gravitational stress during numerical simulation calculations using UDEC discrete element software, and the location of the application was at the shell hole of the first stage of the slope. In order to study the law of dynamic response of the slope under the blast load, some nodes were selected in the model for tracking and monitoring.

The locations of the nodes are shown in Fig. 3. Where the measurement point numbers are 1-4# along the slope from bottom to top, respectively.

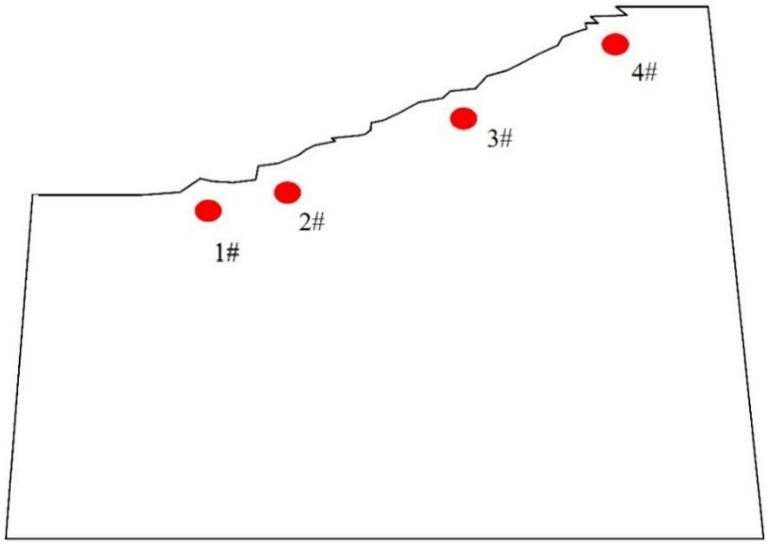

Figure 3 The location of the measurement in the model

The study area is divided into Ⅰ area and Ⅱ area. Among them, the 6-6′ profile of the north gang was selected for numerical simulation calculation in Area Ⅰ, and the 9-9′ profile of the east gang was selected for numerical simulation calculation in Area Ⅱ.

The model monitoring points are set up a total of four, and all located in the slope surface, mainly for monitoring the slope stress process. The calculation gets the results of the stress time course curve of the monitoring points.

Check point 1#, 2# in the horizontal direction of the stress time-symmetric curve shown in Figure 4, it can be seen in the input blasting load, check point 1# slope in the horizontal direction after 0.81-1.7s the stress curve tends to zero.

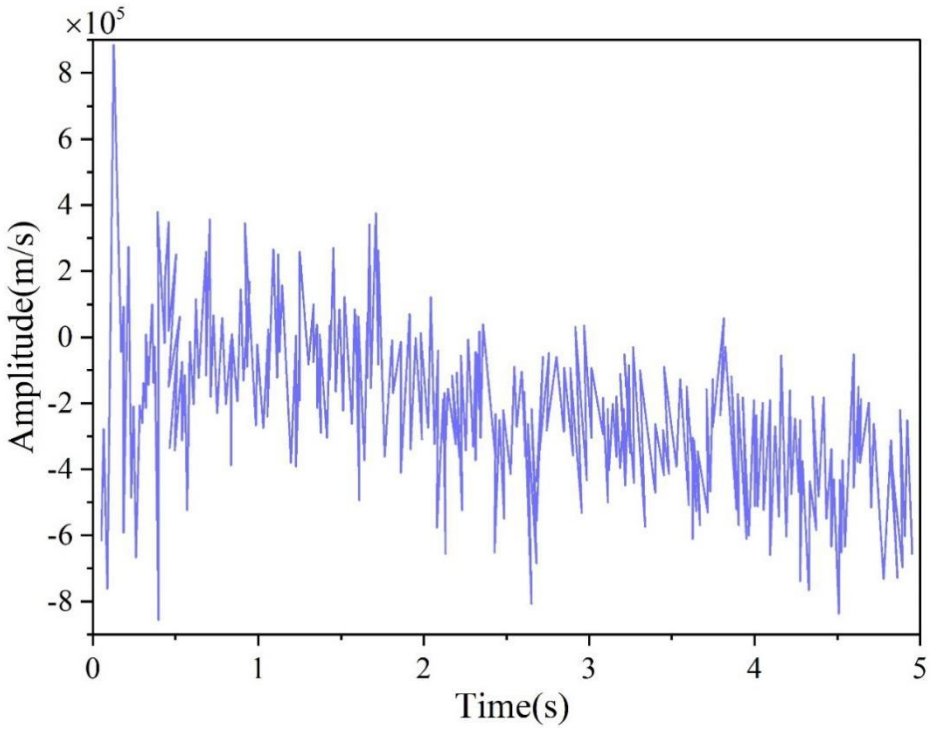

(a) 1#

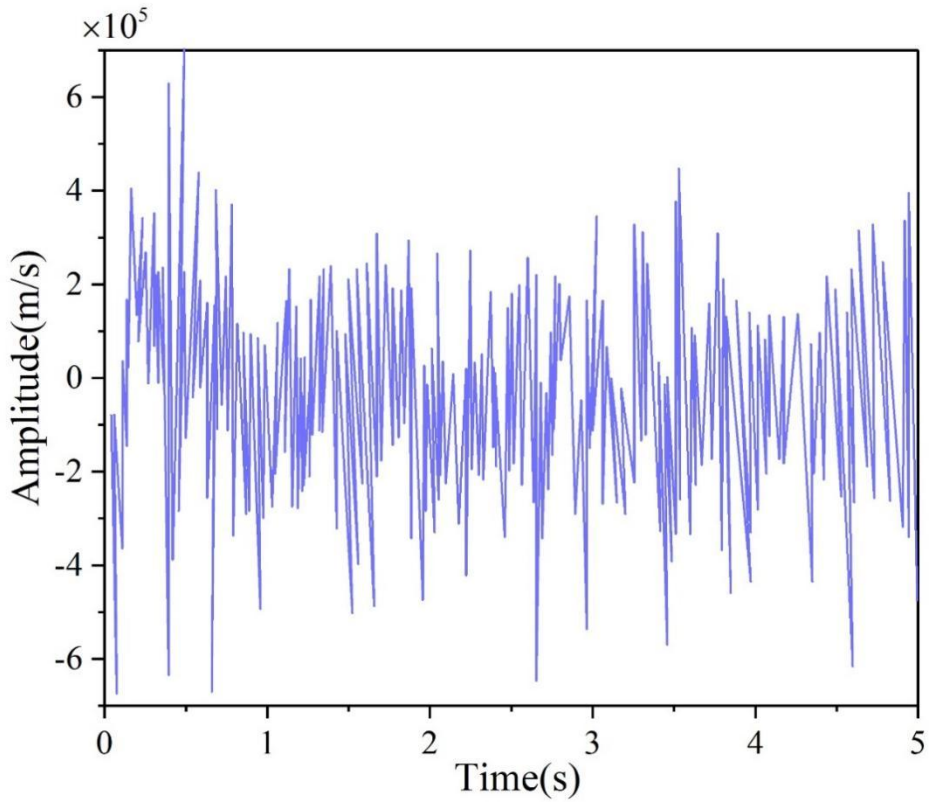

(b) 2#

Figure 4 In the horizontal direction, the curve is called

The vertical stress time curve is shown in Fig. 5. It can be seen that after

inputting the blasting load, the vertical stress curves of the slopes at checkpoints 1# and 2# tend to zero after 0.73-1.4s, indicating that the slopes reach the equilibrium state after 0.73-1.4s under the blasting condition.

Comprehensive check point 1 #, 2 # in the horizontal direction of the stress curve, can be derived from the blasting vibration duration of about 0.73-1.4s, which also coincides with the duration of the field blasting vibration test obtained. 1 and 2 monitoring points, the initial stress is larger, which indicates that the seismic wave generated by the loose blasting on the foot of the slope has a certain effect, and the stress at the foot of the slope to reach the maximum value.

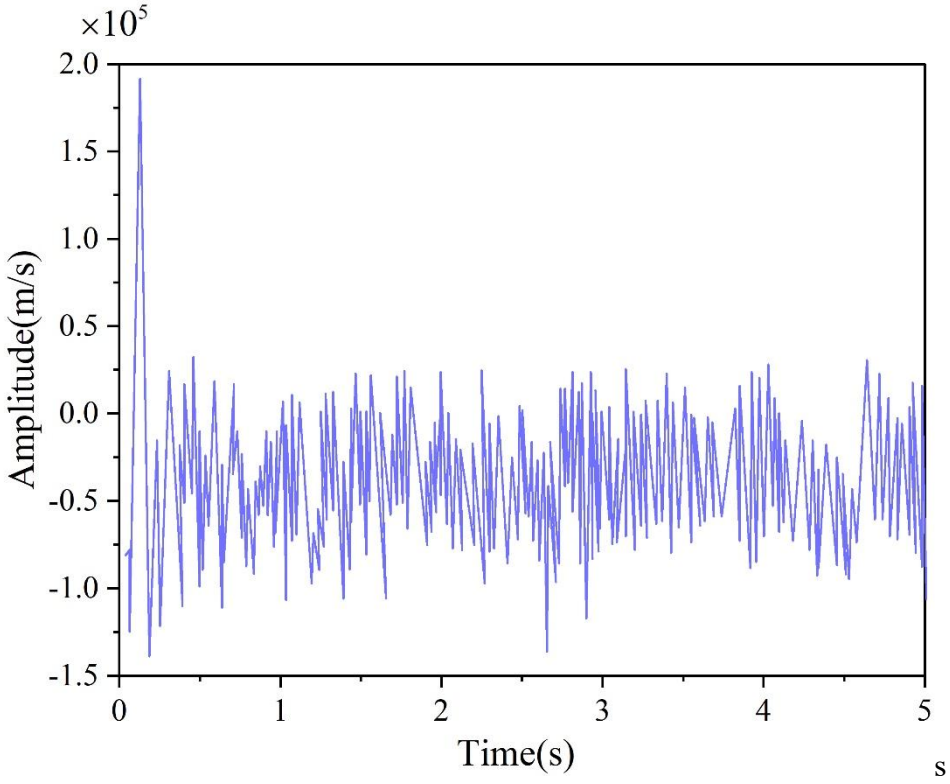

(a) 1#

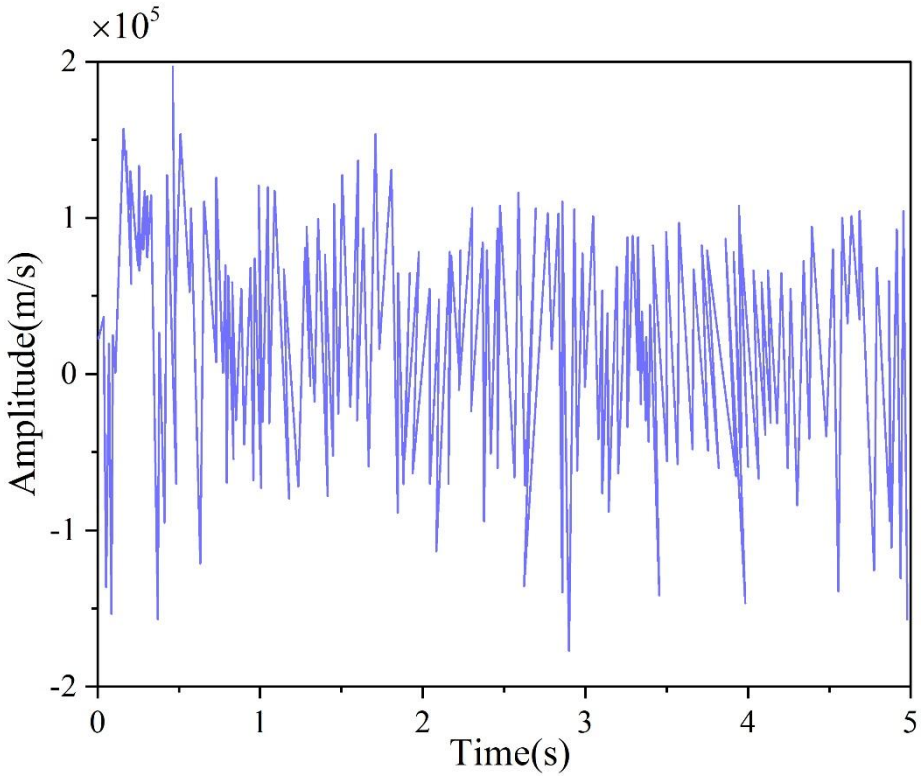

(b) 2#

Figure 5 Vertical stress interval curve

4.6 Sensitivity analysis

Numerical calculations were performed using the dynamics Quake/W module of Geostudio finite element software. The blasting signals entered in this case were the four measured blasting vibration data during the production blasting. These four blasting vibration signals were coded 1#~4# to distinguish the signals.

The time-range curves of the mass vibration velocity of 1#~4# vibration signals are shown in Figure 6.

The peak values of the mass vibration velocity of 1#, 2#, 3# and 4# signals are 56.31 mm/s, 73.26 mm/s, 42.11 mm/s and 56.79 mm/s, respectively, and the main frequency of vibration is 42.15 Hz, 24.09 Hz, 50.48 Hz and 52.13 Hz, respectively.

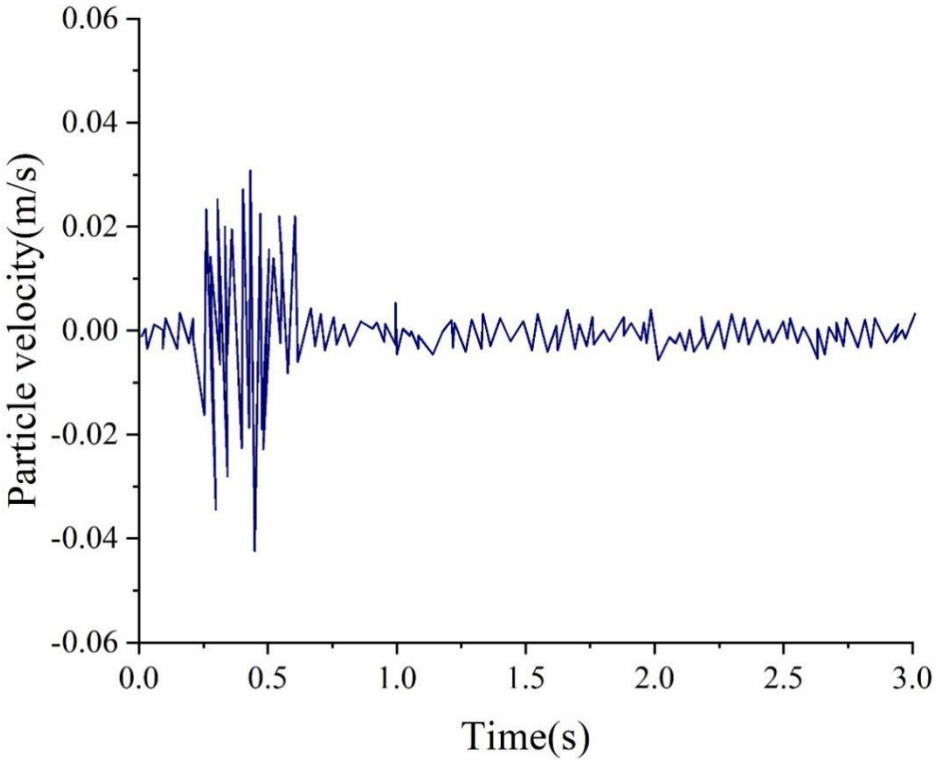

(a) 1# signal point vibration curve

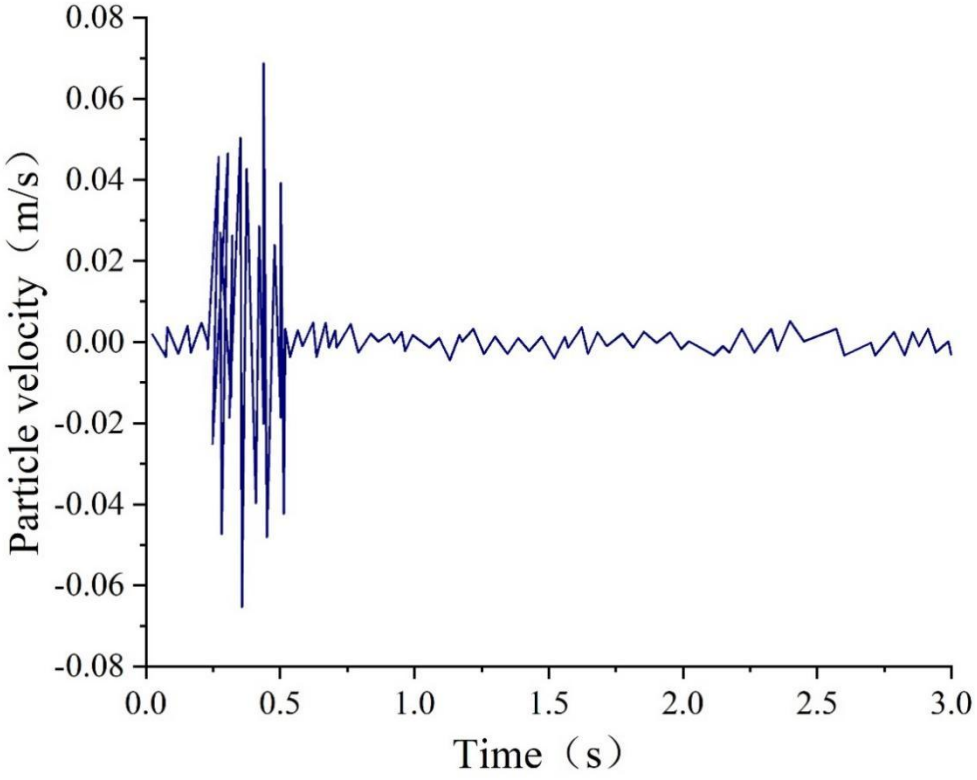

(b) 2# signal point vibration curve

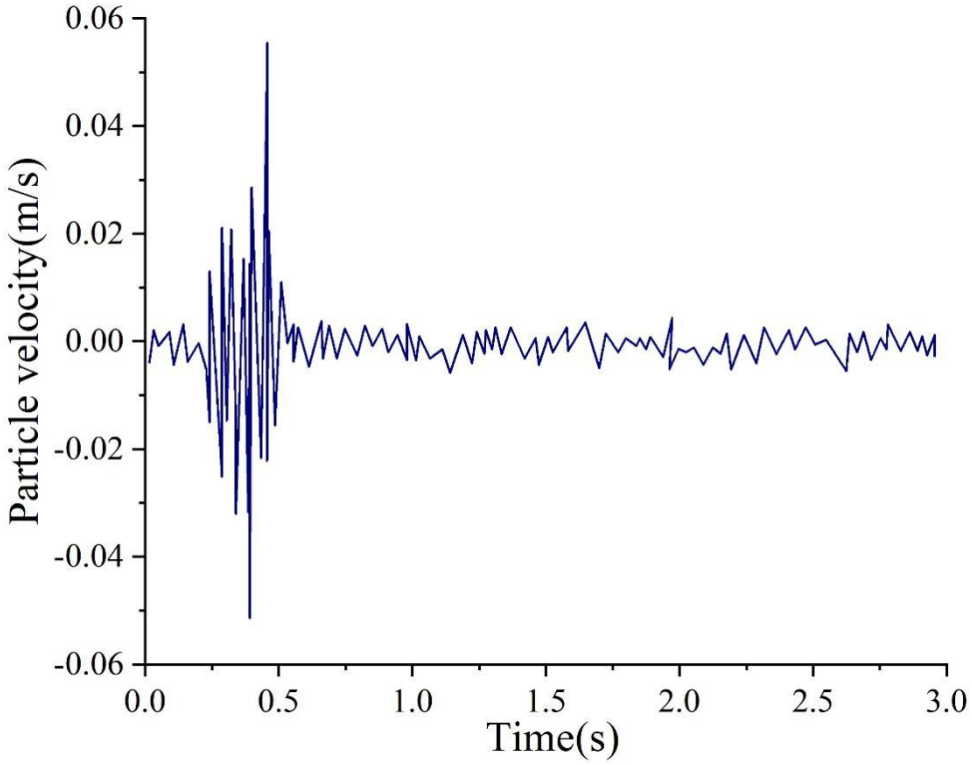

(c) 3# signal point vibration curve

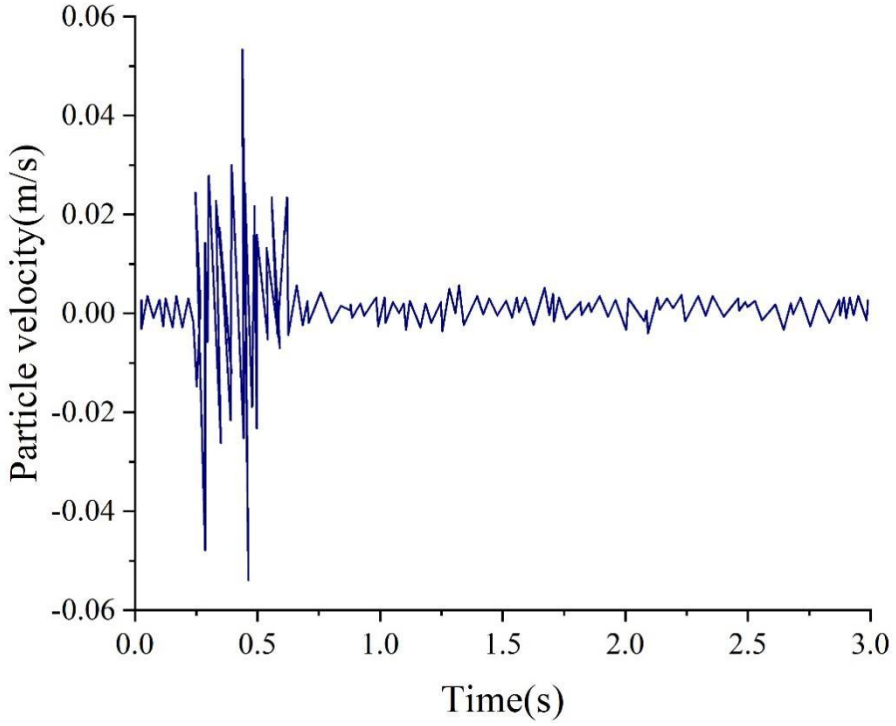

(d) 4# signal point vibration curve

Figure 6 The time curve of the vibration velocity of the 1# ~ 4# vibration signal

The 1#~4# vibration signals were imported into the dynamics Quake/W module of Geostudio finite element software for vibration calculation, and then the results

were imported into the Slope/W module to calculate and analyze the stability of the slope, and the stability coefficients of the slope were obtained. Substitute 1#~4# vibration signals to calculate the stability bar diagram and stability coefficient time trend.

After substituting 1#~4# vibration signals into the calculation, their minimum safety coefficients appear in 0.29s, 0.41s, 0.52, 0.64s. The corresponding minimum safety coefficients are Fs=1.25, Fs=1.37, Fs=0.94, Fs=0.68, respectively.

Comparing 1# (56.31 mm/s, 42.15 Hz) and 2# signals (73.26 mm/s, 24.09 Hz), it can be seen that the plasmonic vibration of 2# signals is stronger than that of 1# signals, but the main vibration frequency of 1# signals is much higher than that of 2# signals. The minimum safety coefficients of 1# and 2# signals are calculated to be 1.25 and 1.37, respectively.The signal with small vibration intensity, on the contrary, has more destructive intensity to the slope. It is concluded that in these two signals, the frequency is the dominant factor in destroying the slope.

Comparing 3# signal (42.11mm/s, 50.48Hz) and 4# (56.79mm/s, 52.13Hz), it can be seen that the dominant frequency of the two signals is basically the same, but the vibration intensity of 4# is large. The minimum safety coefficients of the signals of 3# and 4# are 0.94 and 0.68, respectively. The signals with large vibration intensity have more destructive intensities for the slopes. It is concluded that when the vibration frequency is similar, the intensity of mass vibration is the dominant factor in destroying the slope.

From the above two comparisons, it can be seen that the destruction of the slope is not only related to the mass vibration intensity but also related to the vibration frequency. When the frequency of the vibration signal is so low that it is similar to the intrinsic frequency of the rock body, then the frequency is the dominant damage factor.

1 # ~ 4 # vibration signals of the safety factor time change trend, it can be seen that the final stabilization of the safety factor are smaller than the signal loading starting point of the safety factor. It indicates that under the action of blasting loading, the phenomenon of cumulative damage occurs in the engineering rock body.

4.7 Slope Stability Evaluation and Prediction

According to the size of the slope stability coefficient, the stable state in which the slope is located can be determined, and its division standard is shown in Table 4. The stable state of the slope is divided into four grades, which are unstable (F≤1.00), unstable (1.00<F≤1.05), basic stable (1.05<F≤1.15), and stable (F≥1.15).

Table 4 Slope stability state division

Slope stability coefficient	F≤1.00	1.00<F≤1.05	1.05<F≤1.15	F≥1.15
Slope stability	Instability	Understability	Basic stability	Stabilization

As a result, combined with the results of stability calculations, the state of the slopes in the study area can be evaluated and predicted. The stable state of each slope is shown in Table 5. Condition Ⅰ (self-weight), Condition Ⅱ (self-weight + blasting).

The slope state prediction takes into account that the safety and stability of the slope is not only related to the topographic and geological conditions, but also related to the construction program, especially related to the blasting technology and blasting program used. Blasting excavation not only changes the original topography, overburden and constraints at the foot of the slope. With the change of spatio-temporal conditions, the slope structure and the mechanical relationship between each other change. Moreover, the seismic inertia force generated by the vibration action of the blasting dynamic load also has a certain adverse effect on the slope stability. Due to the frequent action of blasting vibration makes the original cracks and laminae of the rock body to produce expansion or misalignment, which reduces the shear energy of the structural surface of the rock body and decreases the frictional resistance. In this paper, we mainly consider the impact of blasting vibration on slope stability is mainly manifested in the repeated action of blasting vibration load leads to the foot of the slope at the rock structural surface of the shear strength

parameter reduction and blasting vibration inertia force of the action of the slope body as a whole downward force increases leading to the dynamic instability of the slope in two aspects.

Under the action of blasting load (Case Ⅱ), the rock body in Area Ⅰ is in an unstable state, and Area Ⅱ is in a stable state. Compared with the slope stability coefficient in the natural state, the reduced stability coefficient predicted in this paper is mainly manifested in the stress concentration area at the foot of the slope.

Table 5 The stability of the slope of each quarry

Slope zoning		Slope stability calculation section		
		Section number	Coefficient of stability	
			Operating condition Ⅰ	Operating condition Ⅱ
Ⅰ Region	North gang	6-6′	Basic stability	Understability
Ⅱ Region	Eastern section	9-9′	Stabilization	Stabilization
	Western section	3-3′	Stabilization	Stabilization

5. Conclusion

This paper focuses on analyzing the influence of vibration load on slope stability by combining the relevant factors affecting slope deformation. The finite element strength reduction method is chosen to analyze the stress time course of slope monitoring points, and the comprehensive evaluation of slope stability in the study area is carried out by combining the results of the sensitivity analysis of the factors affecting the stability of slopes under vibratory loading.

Analyze the structural surface shear strength parameters of the slopes in the study area and update the original geomorphological measurement data of the slopes. Simulating the input vibration load, the slope checkpoints 1# and 2# converge to zero after 0.73-1.4s in the horizontal direction and vertical direction stress curve. It indicates that the slope reaches the equilibrium state after 0.73-1.4s under the blasting condition, and the duration of blasting vibration is about 0.73-1.4s.

Calculate the minimum safety coefficient of 1 # ~ 4 # vibration signal and the corresponding minimum safety factor. 1 #, 2 # vibration signal comparison found that the 2 # signal of the mass vibration than the 1 # signal, but the 1 # signal main vibration frequency is much higher than the 2 # signal. 1 #, 2 # signal of the minimum safety factor of 1.25 and 1.37, respectively. Vibration strength of the small signal, but the destruction of the slope intensity is greater! The signal with small vibration intensity, on the contrary, has more destructive intensity to the slope. Corresponding the monitoring points in the actual area of the slope, study Ⅰ area in the case of blasting vibration loading appears in an unstable state. Study Ⅱ area is in a stable state. And it is predicted that the reduced stability coefficient of the slope is mainly manifested in the stress concentration area at the foot of the slope.

References

[1] Khajehzadeh, M., Taha, M. R., Keawsawasvong, S., Mirzaei, H., & Jebeli, M. (2022). An effective artificial intelligence approach for slope stability evaluation. Ieee Access, 10, 5660-5671.

[2] Qi, C., & Tang, X. (2018). Slope stability prediction using integrated metaheuristic and machine learning approaches: A comparative study. Computers & Industrial Engineering, 118, 112-122.

[3] Carrión-Mero, P., Briones-Bitar, J., Morante-Carballo, F., Stay-Coello, D., Blanco-Torrens, R., & Berrezueta, E. (2021). Evaluation of slope stability in an urban area as a basis for territorial planning: A case study. Applied Sciences, 11(11), 5013.

[4] Kamal, A. M., Hossain, F., Ahmed, B., Rahman, M. Z., & Sammonds, P. (2023). Assessing the effectiveness of landslide slope stability by analysing structural mitigation measures and community risk perception. Natural Hazards, 117(3), 2393-2418.

[5] Koopialipoor, M., Jahed Armaghani, D., Hedayat, A., Marto, A., & Gordan, B. (2019). Applying various hybrid intelligent systems to evaluate and predict slope

stability under static and dynamic conditions. Soft Computing, 23, 5913-5929.

[6] YANG, T., WANG, H., DONG, X., LIU, F., ZHANG, P., & DENG, W. (2020). Current situation, problems and countermeasures of intelligent evaluation of slope stability in open pit. Journal of China Coal Society, 45(6).

[7] Kumar, P. R., Muthukkumaran, K., & Sharma, C. (2024). Technological Advancements and Sustainable Practices in Rock Slope Stability–Critical Review. Physics and Chemistry of the Earth, Parts A/B/C, 103699.

[8] Qi, S., Ling, D., Yao, Q., Lu, G., Yang, X., & Zhou, J. W. (2021). Evaluating slope stability with 3D limit equilibrium technique and its application to landfill in China. Engineering Geology, 280, 105939.

[9] Tao, Z., Zhu, C., Zheng, X., & He, M. (2018). Slope stability evaluation and monitoring of Tonglushan ancient copper mine relics. Advances in Mechanical Engineering, 10(8), 1687814018791707.

[10] Wang, Z. Y., Gu, D. M., & Zhang, W. G. (2020). Influence of excavation schemes on slope stability: a DEM study. Journal of Mountain Science, 17(6), 1509-1522.

[11] Du, S. G., Saroglou, C., Chen, Y., Lin, H., & Yong, R. (2022). A new approach for evaluation of slope stability in large open-pit mines: a case study at the Dexing Copper Mine, China. Environmental Earth Sciences, 81(3), 102.

[12] Hoang, N. D., & Bui, D. T. (2017). Slope stability evaluation using radial basis function neural network, least squares support vector machines, and extreme learning machine. In Handbook of neural computation (pp. 333-344). Academic Press.

[13] Mishra, M., Gunturi, V. R., & Miranda, T. F. D. S. (2019). Slope stability analysis using recent metaheuristic techniques: A comprehensive survey. SN Applied Sciences, 1(12), 1674.

[14] Zhang, J., & Li, J. (2021). A comparative study between infinite slope model and Bishop's method for the shallow slope stability evaluation. European Journal of Environmental and Civil Engineering, 25(8), 1503-1520.

[15] Morante, F., Aguilar, M., Ramírez, G., Blanco, R., Carrión, P., Briones, J., & Berrezueta, E. (2019). Evaluation of slope stability considering the preservation of the general patrimonial cemetery of Guayaquil, Ecuador. Geosciences, 9(3), 103.

[16] TASSAR PANA,JUMRIK TAIPODIA,PHURBA DORJEE PHILLEY & ADITYA KUMAR ANSHU. (2024). Landslide hazard vulnerability assessment using surface wave method coupled with slope stability analysis: a case study. Sādhanā(3),229-229.

[17] Kenue Abdul Waris,Sheikh Junaid Fayaz,Alluri Harshith Reddy & B. Munwar Basha. (2024). Pseudo-static slope stability analysis using explainable machine learning techniques. Natural Hazards(prepublish),1-33.

[18] Pooneh Shah Malekpoor,Susana Lopez Querol & Sina Javankhoshdel. (2024). Pseudo-static approach for slope stability analysis within a stochastic probabilistic framework for moderate earthquakes. Soil Dynamics and Earthquake Engineering108846-108846.

[19] Jingchao Guan,Baoluo Zheng,Yalan Li,Wei Zhao & Xilu Zhao. (2024). Research on Bifurcated Origami Hydraulic Dampers for Real Road Vibration Loads. Applied Sciences(14),6374-6374.

[20] M Arnold,S Filopoulos,W White & M Kamruzzaman. (2024). A semi-empirical model for time-domain tower Vortex induced Vibration load simulations of wind turbines. Journal of Physics: Conference Series(2).